Materials Science & Engineering C 131 (2021) 112478

Contents lists available at ScienceDirect

Materials Science & Engineering C

journal homepage: www.elsevier.com/locate/msec

Mechanically tunable photo-cross-linkable bioinks for osteogenic differentiation of MSCs in 3D bioprinted constructs

Meenakshi Kamaraj [a,1], Gaddamedi Sreevani [a,1], Ganesan Prabusankar [b], Subha Narayan Rath [a,*]

[a] Regenerative Medicine and Stem cell Laboratory (RMS), Department of Biomedical Engineering, Indian Institute of Technology Hyderabad, Telangana, India
[b] Organometallic Chemistry Laboratory, Department of Chemistry, Indian Institute of Technology Hyderabad, Telangana, India

ARTICLE INFO

Keywords:
3D bioprinting
Osteogenesis
Hydrogel
Photo-cross-linkable bioink
Material stiffness

ABSTRACT

3D bioprinting technique renders a plausible solution to tissue engineering applications, mainly bone tissue regeneration, which could provide the microenvironment with desired physical, chemical, and mechanical properties. However, the mechanical and structural stability of current natural polymers is a critical issue in the fabrication of bone tissue-engineered scaffolds. To overcome these issues, we have developed 3D bioprintable semi-synthetic polymers derived from natural (sodium alginate, A) and synthetic (polyethylene glycol, PEG) biopolymers. In order to enhance the cross-linking properties and biocompatibility, we have functionalized these polymers with acrylate and methacrylate chemical moieties. These selected combination of natural and synthetic polymers improved the mechanical strength due to the synergistic effect of covalent as well as ionic bond formation in the hydrogel system, which is evident from the tested tensile data. Further, the feasibility of 3D bioprinting of acrylate and methacrylate functionalized PEG and hydrogels have been tested for the biocompatibility of the fabricated structures with human umbilical cord mesenchymal stem cells (UMSCs). Further, these bioprinted scaffolds were investigated for osteogenic differentiation of UMSCs in two types of culture conditions: namely, i) with osteoinduction media (with OIM), ii) without osteoinduction media (w/o OIM). We have examined the osteoinductivity of scaffolds with the activity of alkaline phosphatase (ALP) content, and significant changes in the ALP activity was observed with the stiffness of developed materials. The extent osteogenic differentiation was observed by alizarin red staining and reverse transcription PCR analysis. Elevated levels of ALP, RUNX2 and COL1 gene expression has been observed in without OIM samples on week 1 and week 3. Further, our study showed that the synthesized alginate methacrylate (AMA) without osteoinduction supplement with young's modulus of 0.34 MPa has a significant difference in ALP quantity and gene expression over the other reported literature. Thus, this work plays a pivotal role in the development of 3D bioprintable and photo-cross-linkable hydrogels in osteogenic differentiation of mesenchymal stem cells.

1. Introduction

Bone tissue engineering gained popularity on addressing the alternate treatment methods to treat defective bone site using biofabrication of three dimensional (3D) implants [1–4]. Tissue-engineered scaffolds consist of biomaterials, cells, and bone-specific growth factors that can substitute the diseased area and promote the bone healing process [2,3]. Osteogenesis in a bone defect site remains a challenge due to its high load-bearing capacity and vascularity [1,2]. Autografts and allografts have been widely used to repair diseased bone and, however, fail due to poor tissue integration, donor site morbidity, and insufficient bone volume in case of large-sized defects. These clinical disputes led to the development of 3D scaffolds that resembles the bone structure with the use of biomaterial and cells [3,4]. To mimic the complex nature of the bone, researchers recently attempted to develop a biomaterial for the supportive nature of bone and cell metabolism for the proper bone tissue growth. Various 3D scaffold fabrication techniques have been widely used to develop bone implants/scaffolds by phase separation methods, freeze-drying, electrospinning, solvent-casting, and salt-leaching. These methods preclude control over the 3D architecture, cell distribution, and

* Corresponding author at: RMS Lab, Department of Biomedical Engineering, Indian Institute of Technology Hyderabad (IITH), Kandi (V), Sangareddy (M), Medak District, 502 285 Telangana, India.
E-mail address: subharath@bme.iith.ac.in (S.N. Rath).
[1] Authors share equal contribution to the study.

https://doi.org/10.1016/j.msec.2021.112478
Received 19 April 2021; Received in revised form 28 September 2021; Accepted 1 October 2021
Available online 16 October 2021

contours of the scaffold [5]. These above-stated confinements can be improved by the rapid prototyping method, which is the extrusion-based 3D bioprinting technique that allows the use of biomaterial with cells to print the desired structure. The in-demand structure can be obtained from computer-aided design (CAD) modeling or the patient-specific clinical data such as magnetic resonance imaging (MRI) and CT-scan [6].

Presently, 3D bioprinting is an emerging area of current interest to scientists. This rapid prototyping technology allowed the fabrication of 3D scaffolds with precise architecture and controlled delivery of cell-laden bioink [7]. The reason for the increasing popularity of 3D bioprinting is its high potential to construct tissues, organs, and other biological systems *in vitro* that mimic their native counterparts [8]. The advocated 3D bioprinting technique enables the construction of tissue-engineered 3D artificial bone by layer-by-layer deposition of osteogenic cells and bone-specific growth supplements at a particular spatial arrangement [9,10]. Mainly 3D bioprinting process uses hydrogel materials since it can encapsulate the cells inside the polymer network to provide a supportive environment and protects from external damage [11]. Hydrogels are natural or synthetic polymeric compounds that can swell by absorbing water. The high-water content of hydrogels makes them biocompatible to living systems and thus received significant interest by the scientific community in recent years for biomedical applications such as biosensors, drug delivery and tissue engineering *etc.* Hydrogels are commonly used materials for bio-inks in 3D bioprinting as they resemble the extracellular matrix surrounding the cells [12]. These hydrogels can be cross-linked by using different cross-linking agents to obtain complex 3D tissue-like scaffolds.

Majorly hydrogel materials are used for extrusion-based 3D bioprinting for the tissue engineering application. Polyethylene glycol (PEG) and sodium alginate (A) are Food and Drug Administration approved materials and widely investigated for tissue regeneration. PEG has a significant advantage of reduced immunological reactions, non-toxicity, and high mechanical strength [13,14] whereas alginate exhibits better biocompatibility and the ability to form hydrogel or formulation of extrudable gel for 3D printing [13,15,16]. These polymers can be easily modified or functionalized, which makes them an ideal material for 3D printing [17–19]. The critical drawback of alginate based bioink need to be printed in a calcium chloride ($CaCl_2$) solution bath or mixed with $CaCl_2$. Both the procedures are cumbersome, either reduces the structure fidelity or blocks the extruder needle [20]. These pronounced confinements pave the way to research more on cross-linking methods. Eventually, photo-cross-linking gained attention in the function of cross-linkers with the help of a photoinitiator and induction of light [21]. In a photoinduced cross-linking strategy, chemical modification of polymer will be devised to enhance the cross-linking parameters and biocompatibility. In general, the formulation of photo-cross-linkable polymers can be achieved by functionalizing them with acrylic or methacrylic group. The formulated polymer with photo-initiator upon exposure to UV/blue light makes hydrogel solidify and preserve the integrity of the prototype. The use of blue light photo-initiators such as LAP, riboflavin, and camphorquinone utilizes a visible light spectrum to photo-cross-link. It can encapsulate cells effectively with high cell viability and has a potential advantage in tissue engineering applications [22,23]. These photo-cross-linked hydrogel scaffolds depict increased mechanical strength and shape fidelity. The photo-cross-linking mechanism, along with 3D bioprinting will enhance structure accuracy and printability.

The mechanical behavior of the hydrogels can be modulated by choice of polymer, polymer concentration and cross-linking mechanism [24]. Matrix stiffness emerged as a primal mechanical cue in stem cell behavior. It plays a vital role in cell phenotype and regulating cell functions. Stem cells differentiate and initiate the tissue development process by communicating with the mechanical cues present in their microenvironment [25,26]. Brain tissue which is one of the soft tissues has tissue elasticity of ~1 kPa and modulus of hard tissues range from 100 kPa to 15 MPa for bone. Researchers attempt to understand the complexity of mechanical interactions with cells using various polymer compositions [25,27]. Rene et al., demonstrated that elastic modulus in the range of 4 MPa depicted osteo differentiation of MSCs. Elastic modulus of the material was altered using methyl acrylate and methyl methacrylate with polyethylene glycol dimethacrylate [28]. Yufan et al., used 3D bioprinted alginate-gelatin scaffolds to study the stiffness-induced cell differentiation. Young's modulus of 225 kPa supported osteogenic differentiation [29]. From the reported studies, matrix stiffness varies with polymer, functional moiety, and type of cross-linker.

However, numerous headways need to develop a composite material and test their applicability for 3D printing and evaluate the scaffolds. To overcome the issues associated with hydrogel materials, we propose to develop hydrogel materials of semi-synthetic polymers that could be used with different materials for 3D bioprinting. In our study, we mainly focused on the material property to re-formulate them to enhance bone tissue regeneration using 3D bioprinting. We hypothesize that the known biopolymers such as PEG and sodium alginate could be modified to make them photo-cross-linkable using acrylate and methacrylate functional groups, which could be used for encapsulating MSCs for 3D bioprinting application. Functionalization of polymer alters material stiffness which has positive impact on cell differentiation. We aim to keep the maximum viability of cells in this process by using the visible light range.

2. Materials and methods

All the commercially available reagents were directly used without further purification, and moisture-sensitive reagents were transferred by using syringe-septum techniques. The solvent dichloromethane (DCM) was dried by distillation prior to use.

2.1. Synthesis of polyethylene glycol diacrylate (PEGDA)

PEG (10 g) was dissolved in DCM (20 mL) in a two-neck flask (100 mL) and 3 equiv. of potassium carbonate (K_2CO_3) was added. Next, 3 equiv. acryloyl chloride was dissolved in DCM (1:10 v/v) was added dropwise to the slurry mixture. The reaction was maintained at room temperature under nitrogen for 24 h. The mixture was then filtered to remove the solids (KCl, $KHCO_3$, and unreacted K_2CO_3). The filtrate was evaporated, precipitated twice in diethyl ether, and dried thoroughly in a vacuum [30].

2.2. Synthesis of polyethylene glycol dimethacrylate (PEGMA)

To the PEG (10 g) in DCM (20 mL), 3 equiv. of triethylamine (Et_3N) was added at room temperature and stirred for 15 min. Later, 3 equiv. of methacrylic anhydride was added dropwise and allowed to stir for four days at room temperature. The reaction mixture was filtered through neutral alumina using DCM, and the solvent was evaporated. By adding diethyl ether, it was precipitated and decanted. The precipitate was vacuum dried.

2.3. Synthesis of alginate acrylate (AA)

AA was prepared by dissolving the alginate (A) sodium salt (0.5 g) in DI water (25 mL), after which a 20-fold excess of acryloyl chloride in DCM was added slowly dropwise at 0-5 °C. The pH was maintained at 8–9 with 5 N NaOH. The reaction mixture was allowed to stir at 5 °C for 24 h. The acrylate polymer was precipitated and washed with ethanol. The residue was dissolved in DI water, kept at −80 °C, dried by lyophilization, and stored at −20 °C until further use.

2.4. Synthesis of alginate methacrylate (AMA)

AMA was prepared by following the procedure described by Smeds

et al. [31,32]. In brief, alginate (A) sodium salt (0.5 g) was dissolved in DI water (25 mL) after which a 20-fold excess of methacrylic anhydride was added at 0-5 °C and pH was adjusted to 8–9 with 5 N NaOH. The solution was stirred at 5 °C for 24 h. The methacrylated polymer was precipitated in ethanol and washed with ethanol. The precipitate was dissolved in DI water, kept at −80 °C, dried by lyophilization, and stored at −20 °C until further use.

2.5. Photo-cross-linkable polymer characterization

The functionalization of PEG and alginate were analyzed by Fourier transform infrared spectroscopy (FTIR) and ^{1}H nuclear magnetic resonance (^{1}H NMR) spectroscopy. The presence of functional groups of PEG and alginate were confirmed by using Fourier transform infrared spectrophotometer (8400S, Shimadzu) in transmission mode. Infrared spectra were recorded from 400 to 4000 cm^{-1} using a resolution of 4 cm^{-1}. ^{1}H NMR spectra were recorded on Bruker Avance 400 MHz spectrometer at 295 K using $CDCl_3$ or D_2O as a solvent.

2.6. Human umbilical cord mesenchymal stem cells (UMSCs) procurement and cell culture

The umbilical cord was collected from donor after informed consent. Explant culture method was used for isolation of UMSCs from the umbilical cord which was described previously [33]. The isolated cells were cultured and expanded in flasks containing Dulbecco's Modified Eagle Medium (DMEM/F12) (Lonza, USA) with 10% fetal bovine serum (PAN Biotech, Germany) and 1% penicillin-streptomycin (Lonza, USA) in an incubator at 37 °C and 5% CO_2 with humidified atmosphere. For all the experiments, passage 4–5 cells were used. The media was changed after every second day.

2.7. Bioink preparation and 3D bioprinting

The photo-cross-linkable polymers with photo-initiator of Lithium phenyl-2,4,6-trimethylbenzoylphosphinate (LAP) were dissolved in sterile DI water to prepare the hydrogel, and sodium alginate was mixed with polyethylene glycol group to increase the viscosity. The mixture was stirred at 400 rpm at room temperature to get a printable gel. The optimized compositions and crosslinking parameters are mentioned in Table 1. The bioink was prepared by mixing cells at the concentration of 10×10^6 cells per mL to the hydrogel to get the desired cell density to fabricate the scaffolds. The CAD model was used to design the scaffold structure with desired porosity using Solidworks and slicing software (Repetier-Host). Then the developed cuboidal structure (10 × 10 × 5 mm) was changed to stereolithography file (.stl) for 3D printing. The .stl file was used as a key source in 3D printer (Biobots, Allevi) to fabricate the samples. The prepared bioink was moved to the plastic Luer-lock tip syringe, which was placed in a 3D printer. Pneumatic pressure (15–25 kPa) was applied to dispense the cell-hydrogel bioink. The printed scaffolds were cross-linked initially with blue light with a wavelength of 405 nm for 5 min then with 5% $CaCl_2$ for another 5 min in total cross-linking time of 10 min. The 3D bioprinted structures were cultured in a cell-specific medium and incubated at 37 °C with 5% CO_2, and media change was carried out every two days. Experiments were performed with and without osteoinduction media (OIM) for all four groups. Fabricated scaffolds were osteogenically induced with osteoinduction media consists of 10 mM of β-glycerophosphate (Sigma-Aldrich, USA), 100 nM of dexamethasone (HiMedia, India) and 50 μg/mL L-Ascorbic acid (HiMedia, India). Cell culture work and 3D bioprinting were carried out in the BSL-2 laminar flow hood. Fig. 1 shows the fabrication of UMSCs encapsulated scaffolds by 3D bioprinting technique.

2.8. Mechanical testing of the 3D printed scaffold

Tensile testing was performed on the 3D printed scaffolds. The influence of cross-linking mechanism was tested to find the mechanical strength of the respective cross-linking agent and the ability to cross-link the hydrogel with different cross-linkers mentioned in Table 2. Dumbbell shape scaffolds were fabricated with 100% infill density based on ASTM D638 standard and used to test the uniaxial tensile strength with the help of the Instron 5900 series. The load of 2 kN was applied with a strain rate of 10 mm/min. The stress-strain curve was plotted with the generated stress and strain data, and Young's modulus was calculated from the stress-strain curve.

2.9. In vitro swelling study of hydrogels

To determine the swelling and degradation behavior of fabricated scaffolds over time, the study has been performed based on a weight ratio. Hydrogels were fabricated as previously specified concentrations and immersed in simulated body fluid (SBF) solution and incubated at 37 °C with the humidified atmosphere. Every two days solution was changed until 21 days of study point. The initial weight of the scaffolds was weighed and noted as (Wi), and after specific time intervals, the swollen samples were blotted and weighted (Wt) [34,35]. The swelling ratio of the hydrogels was calculated according to the formula mentioned below,

$$\text{Swelling percentage} = \frac{Wt - Wi}{Wi} * 100.$$

2.10. Evaluation of cell viability

The viability of the printed scaffolds was evaluated with the use of live/dead staining on day 1, as previously reported. In brief, to perform a live/dead assay, the media from the scaffolds was removed and washed with phosphate buffered saline (PBS), then fluorescein diacetate (FDA) (Invitrogen, USA) with concentration of 2 μg per 1 mL of 1× PBS was added to the scaffolds and incubated at 37 °C for 15 min. After the successful staining of FDA, it was removed, and propidium iodide (PI) (Molecular Probes, USA) of 20 μg per 1 mL of 1× PBS was added to the scaffolds and incubated at 37 °C for 2 min [36]. Live and dead cells

Table 1
Optimized parameters for scaffold fabrication using 3D bioprinting.

	Polyethylene glycol				Alginate	
Functional group	Acrylate		Methacrylate		Acrylate	Methacrylate
Sample code	PEGDA	PEGDA/A	PEGMA	PEGMA/A	AA	AMA
Photo-cross-linkable polymer conc. (% w/v)	20	20	20	20	6	4
Alginate conc. (% w/v)	0	2.5	0	2.5	0	0
LAP (Photo initiator conc.) (% w/v)	0.1	0.1	0.1	0.1	0.1	0.1
$CaCl_2$ (% w/v)	–	5	–	5	5	5
Total crosslinking time (min)	10	10	10	10	10	10

PEGDA: polyethylene glycol diacrylate, PEGDA/A: polyethylene glycol diacrylate + sodium alginate, PEGMA: polyethylene glycol dimethacrylate, PEGMA/A: polyethylene glycol dimethacrylate + sodium alginate, AA: alginate acrylate, AMA: alginate methacrylate, All the samples have photo-initiator of Lithium phenyl-2,4,6-trimethylbenzoylphosphinate (LAP).

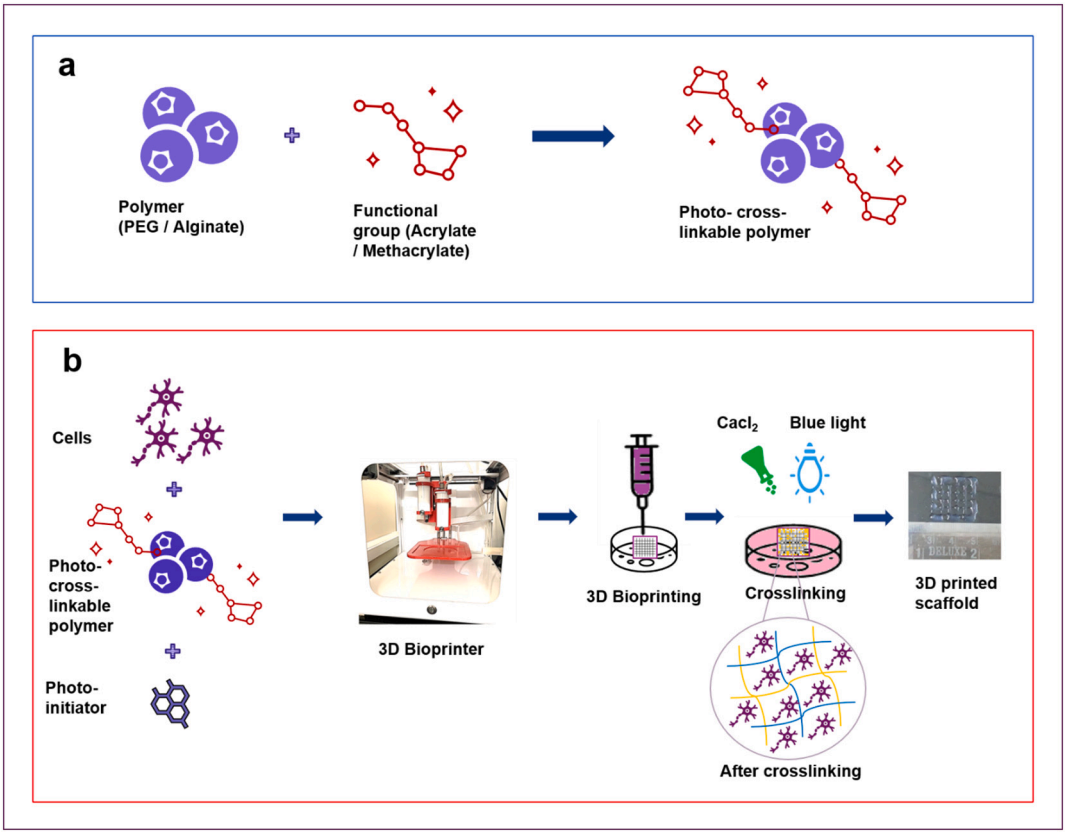

Fig. 1. Schematic diagram of (a) chemical synthesis of photo-cross-linkable polymers (b) overall 3D bioprinting process to fabricate photo crosslinked scaffolds.

Table 2
Two different crosslinking methods and their respective crosslinking ability.

Crosslinking mechanism	PEGDA	PEGDA/A	PEGMA	PEGMA/A	Alginate	AA	AMA
Composition	PEGDA + LAP	PEGDA + Alginate + LAP	PEGMA + LAP	PEGMA + Alginate + LAP	Alginate	AA + LAP	AMA + LAP
Blue light	++	+	++	+	−	−	−
$CaCl_2$	−	+	−	+	++	+	+
Blue light + $CaCl_2$	++	++	++	++	++	++	++

(++ fully crosslinked, + partially crosslinked, − did not crosslink.)

outcomes were observed under a fluorescence microscope (Zeiss Apotome 2) FDA (green color) stain the live cells, and PI (red color) stains the dead cells.

2.11. Cell proliferation assay using Alamar blue

Measurement of cell proliferation was assessed by the alamar blue (alamarBlue™ Cell Viability Reagent, Invitrogen, USA) assay after week 1 and week 3. After removing the media from the scaffolds, 1 mL of alamar blue master mix was added to each scaffold in a well plate. The plate was incubated at 37 °C for 4 h. After the incubation, 100 μL was removed from each well and placed in a 96 well plate with control as AB master mix and media as blank. Absorbance was measured at 570 nm and 600 nm to determine the percentage of AB reduction over time [33].

2.12. DNA quantification by PicoGreen kit assay

To quantify the double-stranded (ds) DNA content of the cells in the scaffold, scaffolds were washed with 1× PBS and treated with lysis buffer (20 mM Tris, pH 7.4, 0.5% v/v Triton X-100, 1 mM EDTA and 100 mM NaCl) as described in our previous work [37]. On week 1 and week 3, cells encapsulated scaffolds were evaluated by measuring dsDNA using a picogreen DNA quantification kit (Quant-iT™ PicoGreen ® dsDNA kit, Invitrogen, USA). The samples fluorescence was measured at 485 nm excitation and 520 nm emission wavelength using micro plate reader.

2.13. Osteogenic differentiation of UMSCs

2.13.1. Evaluation of Alkaline phosphatase (ALP) activity

Alkaline phosphatase (ALP) is a metalloenzyme that is a tissue-specific marker for bone mineralization and expresses the ALP gene marker in osteogenesis studies. A positive result of bone regeneration is measured by robust ALP expression. 3D bioprinted scaffolds were fixed with citrate solution, and diazonium salt solution (Alkaline phosphatase, Sigma-Aldrich, USA) was used to visualize the ALP activity on week 3 without osteoinduction samples. These scaffolds were counterstained with hematoxylin solution and viewed under microscopy and pictures were captured. The acquired images were analyzed using open software ImageJ. ALP assay (ALP assay kit, Sigma-Aldrich, USA) was performed for all the groups to quantify the ALP content as evidence of the staining protocol. The assay was carried out as per the manufacturer's protocol after 3 weeks. In short, the scaffolds were washed with 1× PBS then lysed using lysis buffer. The lysate was incubated with p-nitrophenyl

phosphate, and the resultant color compound was measured at 405 nm in the absorbance wavelength mode using a microplate reader.

2.13.2. Alizarin red staining

Alizarin red staining was performed on week 3 to assess the calcified matrix on 3D bioprinted scaffolds. The fabricated samples were rinsed in 1× PBS solution before being fixed for 10 min in a 10% formalin solution. The fixed samples were stained with 2% alizarin red (HiMedia, India) for 15 min at room temperature. The colored samples were visualized under EVOS M7000 (EVOS M7000, Thermo Fisher Scientific) imaging system for calcium deposits and images were captured.

2.13.3. Gene expression analysis

The osteogenic differentiation genes in the scaffolds were quantified using reverse transcription quantitative PCR (RT-qPCR) analysis. The total RNA content of samples was isolated using the TRIzol reagent (Ambion, Life Technologies, USA). Manufacturer's protocol was followed to perform reverse transcription reaction using Quanti Tect Reverse Transcription Kit (Qiagen) using an isolated pure total RNA (1 μg). Gene expressions of osteogenic markers like ALP, RUNX2 (RUNX Family Transcription Factor 2) and COL1 (type I collagen) were determined using Real-Time PCR Detection System (Bio-Rad Laboratories, USA). To normalize the expression of the target gene, GAPDH was utilized as a reference gene. The primers are listed in Table 2. The results were determined using the $2^{-\Delta\Delta CT}$ method and reported as a fold difference between the test group's gene expression and that of the reference.

2.13.4. Statistical analysis

All experimental comparisons were performed by a one-way analysis of variance (ANOVA) with Tukey's post-hoc test using origin software (OriginPro 9.0). The results were expressed with mean ± standard deviation and a value of $p < 0.05$ considered as statistically significant.

3. Results

3.1. Photo-cross-linkable polymer synthesis and characterization

The properties of the polymers can be manipulated *via* synthetic modification of the polymers, such as the addition of functional groups within or at the end of the polymer or using cross-linking agents. Chemical modification of the polymer and cross-linking provides drastic influence on the properties of the polymer, such as mechanical properties, solubility, and diffusion *etc.* Especially, acrylates are good candidates for chemical cross-linking as they produce radicals for cross-linking in the presence of light and initiator. Hence, the functionalization of polymers with acrylates allows the polymer to undergo covalent cross-linking in the presence of light using an initiator *via* radical mechanism and allows the polymer to retain the shape while 3D printing.

We chose the polymers PEG and sodium salt of alginate for the photo-cross-linking *via* functionalization through acrylation. In this regard, PEG was treated with acryloyl chloride and methacrylic anhydride in the presence of a base to obtain PEGDA and PEGMA, respectively (Fig. 2 (a, b)). The natural polymer, alginate, was acrylated by dissolving the sodium salt of alginate in DI water followed by the addition of acryloyl chloride or methacrylic (Fig. 2 (c, d)).

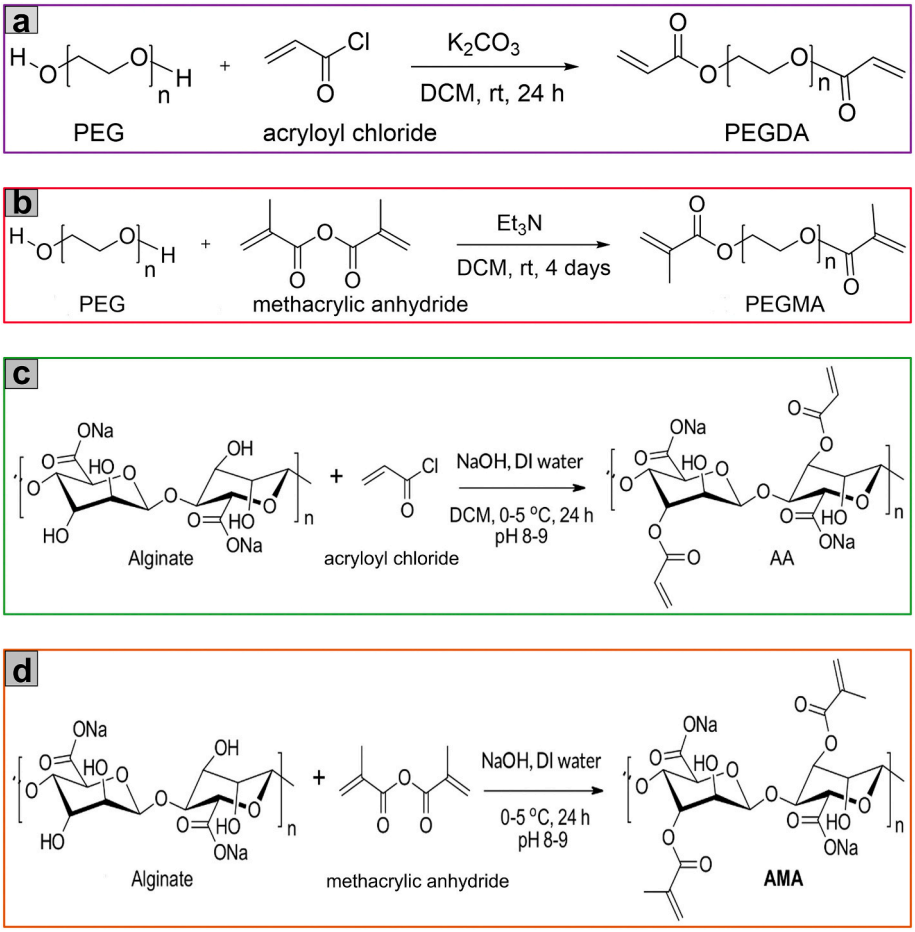

Fig. 2. Acrylate and methacrylate functionalization of polyethylene glycol and sodium alginate (a) PEGDA, (b) PEGMA, (c) AA, (d) AMA.

The functionalization was confirmed by the ^{1}H NMR spectroscopy. As shown in Fig. 3 (a), PEG acrylate protons were observed at 5.8 ppm and 6.1 to 6.4 ppm. The methacrylate group peaks were observed at 5.5 and 6.1 ppm. The methyl protons of methacrylate were observed at 1.9 ppm. Under similar lines, conversion of the alginate to AA and AMA was also confirmed by ^{1}H NMR. As shown in Fig. 3 (b), we can observe that the acrylate protons at 5.6 ppm and in the region of 5.9 to 6.2 ppm for three protons of the acrylate group of alginate. We can also observe that the peaks at 5.3 and 5.6 ppm for the methacrylate group of AMA and the methyl protons of methacrylate was observed at 1.8 ppm. The number averaged molecular weight (Mn) of the polymers were calculated from ^{1}H NMR spectra (Supplementary Table S1). Further, the functionalization of polymers and their chemical moieties were confirmed using FTIR data (Supplementary Fig. S1). The end capping of PEG with acrylate or methacrylate group was confirmed by the FTIR spectra. The intensity of absorption band around 3400 cm^{-1} was reduced in acrylated and methacrylated samples, which is due to the functionalization. It is evident that photo-cross-linkable moiety attaches to the hydroxyl terminal of the polymers. The three signature peaks at 1638, 1283 and 1110–1041 cm^{-1} supports the formation ester linkage by acrylate or methacrylate group with polymers (Supplementary Fig. S1). In particular, the C═O stretching frequency at 1638 cm^{-1} can be ascribed to the presence of α,β, unsaturated ester such as acrylate or methacrylate group.

3.2. Mechanical testing

The dumbbell-shaped scaffolds were fabricated with optimized parameters of all the samples by the 3D printing process. The stress-strain curve was plotted from the data set and Young's modulus was calculated from the stress-strain curve. The stress-strain curve of all the groups was shown with their corresponding Young's modulus (Fig. 4). Fig. 4 (a–d) depicts that the cross-linking mechanism influences the mechanical strength of the hydrogel samples. Dually cross-linked hydrogel materials exhibit higher tensile strength compared with a single cross-linking agent. We could describe that cross-linking with both physical and chemical agents such as blue light and $CaCl_2$ increases the tensile strength of the photo-cross-linkable hydrogels. Further, two differently cross-linked samples were shown in Supplementary Fig. S2. From the stress-strain curve Fig. 4 (e), we observed that AA exhibited high tensile properties than other groups. AA showed stiffer property than other gels with Young's modulus of 0.77 MPa. AMA showed a low Young's modulus of 0.34 MPa, which was flexible when compared with other hydrogels. Both the acrylate functionalized groups such as PEGDA/A and AA demonstrates stiff material properties, while methacrylate groups of PEGMA/A and AMA show flexibility. The PEGDA and Alginate have a tensile modulus of 0.27 and 0.29 MPa, while PEGMA depicts less mechanical strength with 0.09 MPa Young's modulus (Supplementary Fig. S3). From these results, we can say that the AA has a high Young's modulus value compared to PEGDA/A, PEGMA/A, and AMA (Fig. 4 (f)). These results indicated that the functionalized PEG and alginate gels depicted high mechanical strength compared to natural as such materials.

3.3. In vitro swelling study of hydrogels

A swelling study of these photo-cross-linked hydrogels was performed to determine the capacity of water uptake based on sample weight gain. As shown in Fig. 5, the swelling behavior of PEGMA/A was high when compared with the other polymers, which indicates that the water intake by PEGMA/A was comparatively higher. PEGMA/A and PEGDA/A followed a similar pattern of swelling where there was an abrupt change in the initial time point and persisted to stable till 168 h. In the case of the AA group, samples remain unchanged until 36 h and after 36 h gradually absorbed water until 168 h and reduced after 336 h. AMA hydrogels initially showed a decrease in weight due to the shrinking of hydrogels till 36 h. Then they gained their water uptake profile from 36 h to 72 h and remained stable till 168 h and reduced quickly in 336 and 504 h. We could observe that there was a sharp increment in the weight of the samples after the initial time points and reached the plateau over the longer incubation time. These water uptake capacity of these materials showed the appropriate environment for cell survival.

3.4. 3D bioprinting of photo-cross-linkable hydrogels and evaluation of cell viability

The acrylated and methacrylated hydrogels were used for 3D bioprinting. Initially, we have optimized the concentration of various polymers and process parameters for 3D bioprinting. To get better printability, alginate was mixed with photo-cross-linkable polymer precursors and held the shape fidelity (Supplementary Fig. S4). The bioink consists of polymer mixture and desired cell concentration was used to print our self-designed model. The fabricated structure was photo-cross-linked using blue light for 5 min and followed by ionically cross-linked with 5% $CaCl_2$ for another 5 min to stabilize the alginate

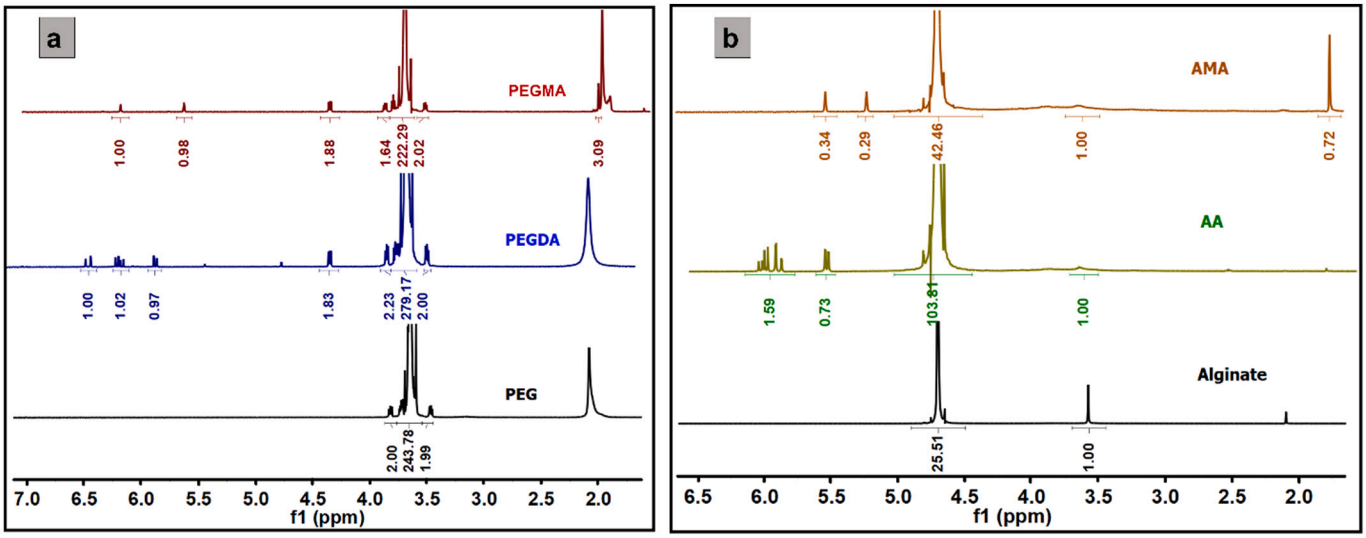

Fig. 3. ^{1}H NMR spectra of (a) Polyethylene glycol group and (b) Alginate group.

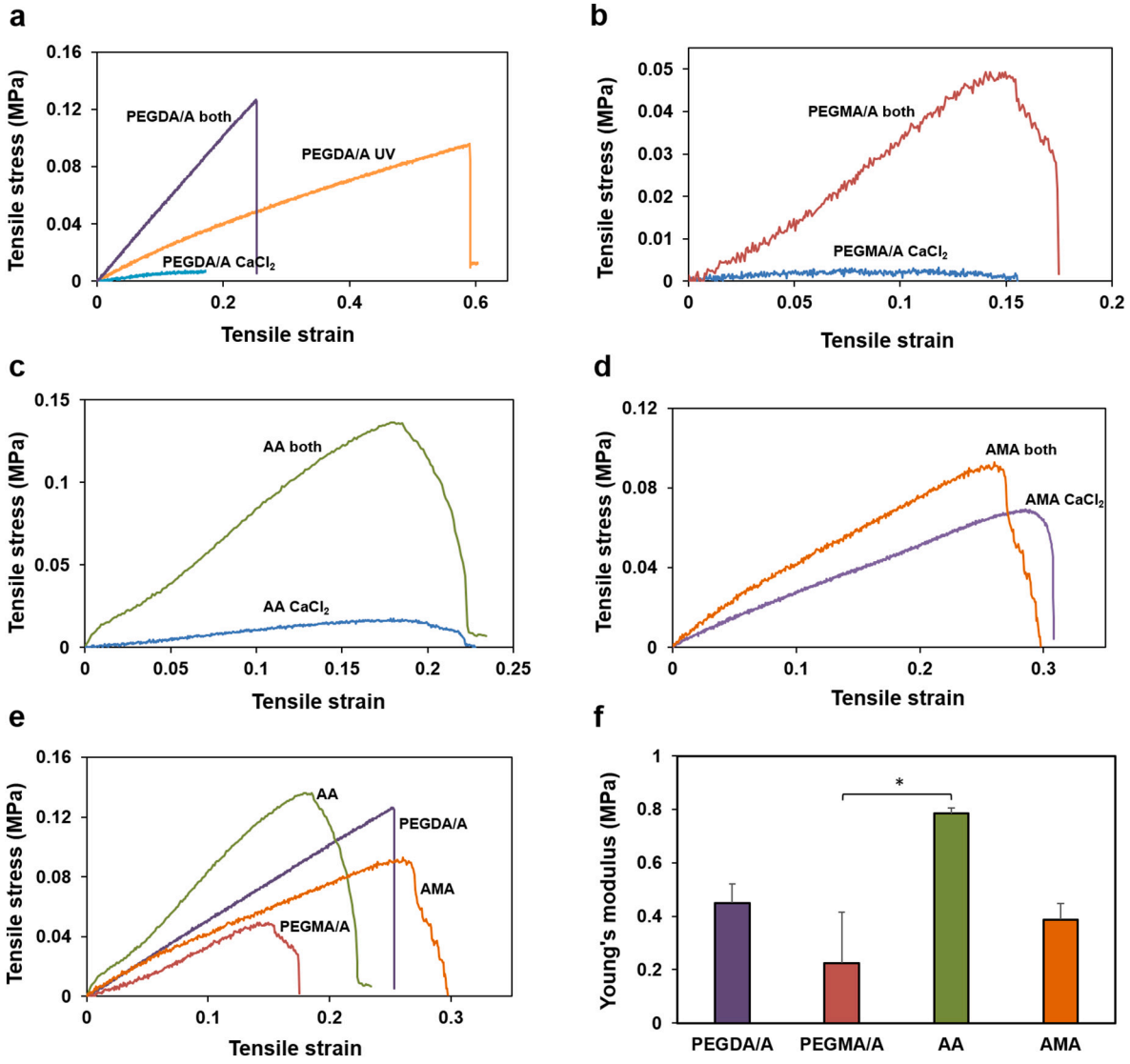

Fig. 4. Tensile test of 3D printed hydrogels (a–d). Stress-strain curve of all the four groups with the different crosslinking mechanism. (e) Stress-strain curve of dual crosslinked samples. (f) Young's modulus (MPa) value of different hydrogels.

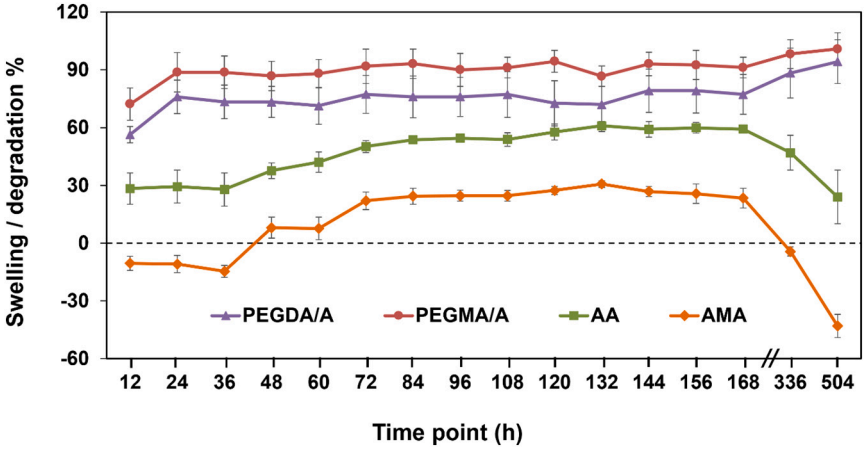

Fig. 5. *In vitro* swelling ability of different hydrogels on various time points.

(Supplementary Fig. S5). The 3D bioprinted scaffolds were cultured in DMEM F/12 complete media with and without osteoinduction supplements until week 3. Further, the fabricated 3D scaffolds were used for cell-based studies.

Primary evaluation of cytocompatibility was performed using live/dead fluorescent staining of FDA/PI on day 1. Bright-field microscopic images (Fig. 6 (a)) showed that cells were distributed homogeneously in the hydrogel system. Fig. 6 (b) indicated the cell viability on various hydrogels; the green color depicts the viable cells in the 3D scaffolds while dead cells stained red. The percentage cell viability was quantified from FDA/PI images using ImageJ which depicts significant cell viability on all the groups (Supplementary Fig. S6). It was found that cells have a

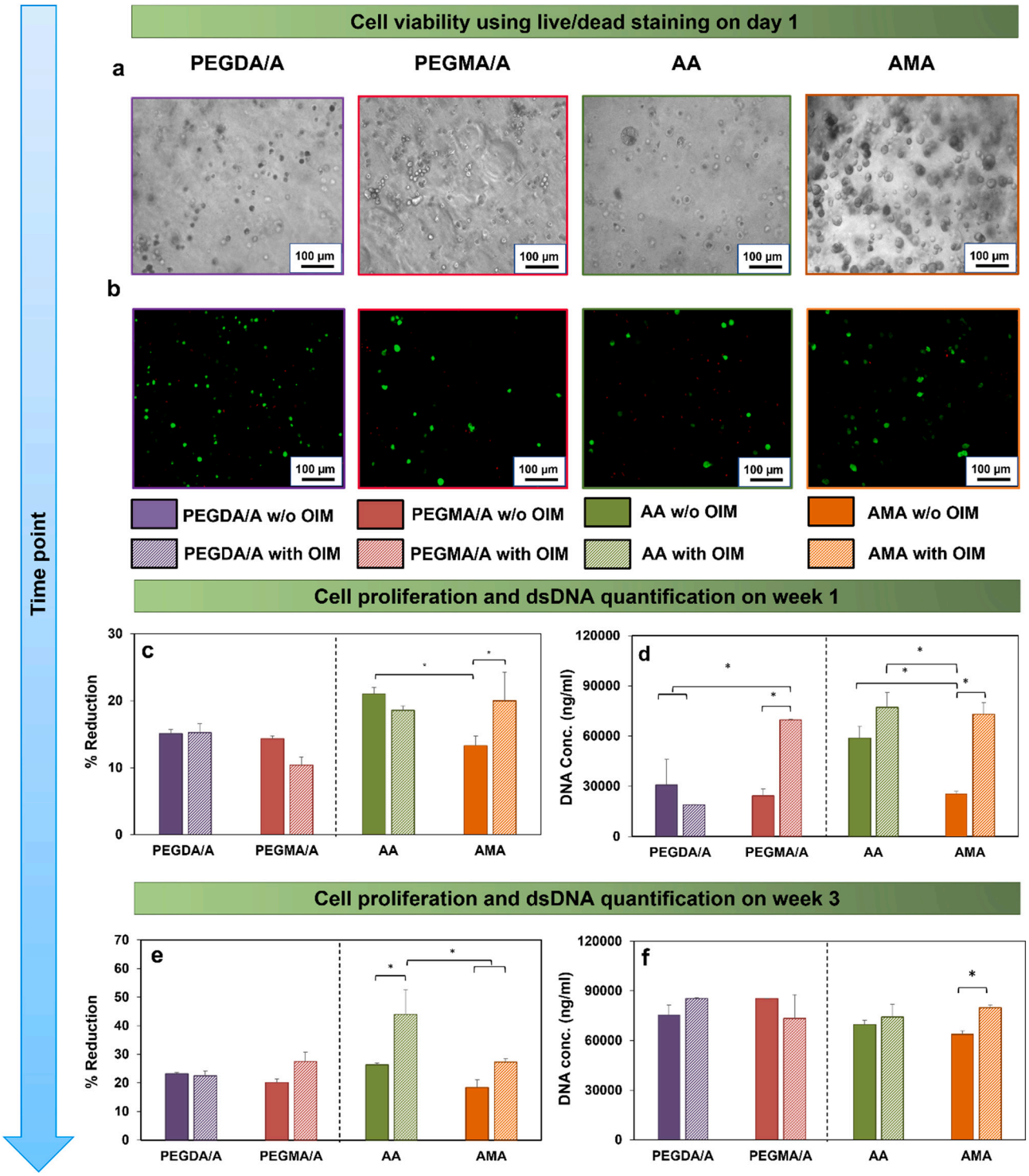

Fig. 6. (a) Light microscope images of 3D bioprinted scaffolds on day 1 shows cells encapsulated in hydrogels. (b) Live/dead fluorescent staining images of photo-cross-linkable hydrogels on day 1 to check the effects of printing parameters. Green fluorescent depicts live cells while red depicts dead cells in the 3D bioprinted scaffolds (a and b: 10× images, scale bar: 100 μm). (c and e) Alamar blue dye reduction assay and (d and f) Quantification of dsDNA content on 3D bioprinted hydrogel scaffolds *with (w)* or *without (w/o)* OIM groups on week 1 (c and d) and week 3 (e and f). * Indicates the significant difference at $p < 0.05$. (For interpretation of the references to color in this figure legend, the reader is referred to the web version of this article.)

circular shape and did not attach as they were encapsulated in the hydrogel.

3.5. Cell proliferation assay using Alamar blue

The metabolic activity of the hydrogel encapsulated cells was analyzed using alamar blue dye reduction assay. The proliferative rate of the cells was evidenced by the reduction of alamar blue at different time points of week 1 and week 3. As shown in Fig. 6 (c) after week 1, the percentage reduction was more in the case of AA without OIM. In contrast, percentage reduction was more in the case of AMA with OIM. From Fig. 6 (e), we also observed that in the case of AA, the cell proliferation was significantly higher after week 3 with OIM compared to AA without OIM and AMA. On week 1, as well as week 3 PEG group did not show any significant difference between them. However, the percentage reduction of dye in the scaffolds after week 3 was significantly increased compared to week 1.

3.6. DNA quantification by Picogreen kit assay

Further, we have performed a picogreen assay for DNA quantification after week 1 and week 3. The quantification of nucleic acid content is an indicator of cell numbers. As shown in Fig. 6 (d and f), there was an approximately two-fold increase in the cell number in all the scaffolds on week 3 compared to week 1 without OIM. PEGMA/A with osteoinduction supplement depicted significantly increased DNA content as compared to without induction media and PEGDA/A group (Fig. 6 (d)). AA without OIM showed a significantly increased value of DNA content on week 1 when compared with AMA without supplement media. However, AA and AMA without OIM did not show any significant difference, and AMA with OIM showed increased DNA quantity than AMA without OIM sample. Fig. 6 (d and f) depicts that using osteoinduction media, PEGDA/A has shown a threefold increase in DNA quantity from week 1 to week 3; in contrast, it was approximately the same on week 1 and week 3 with other hydrogels. The use of osteoinduction media significantly increased the DNA content of week 1 samples when compared to without induction group. From Fig. 6 (f), we could observe that almost all the groups showed a similar increment while AMA with induction media significantly differed from without OIM.

3.7. Osteogenic differentiation of UMSCs

3.7.1. Evaluation of Alkaline phosphatase (ALP) activity

The osteogenic differentiation of the encapsulated UMSCs in different hydrogels was assessed by ALP staining and assay. The specific ALP activity was measured by analyzing ALP content in the scaffolds on week 3 with and without OIM. From Fig. 7 (a) we could observe that there was no significant difference between PEGDA/A and PEGMA/A while PEGMA/A without induction media showed increased ALP content when compared to samples with OIM. AA with OIM showed increased ALP activity as compared to without OIM, while AMA without osteoinduction sample showed significantly higher values when compared with AMA with OIM. From the alginate group, we could observe that AMA without OIM significantly differs from AA without OIM group. The ALP-stained encapsulated cells were visualized under light microscopy and observed the staining pattern on the scaffolds.

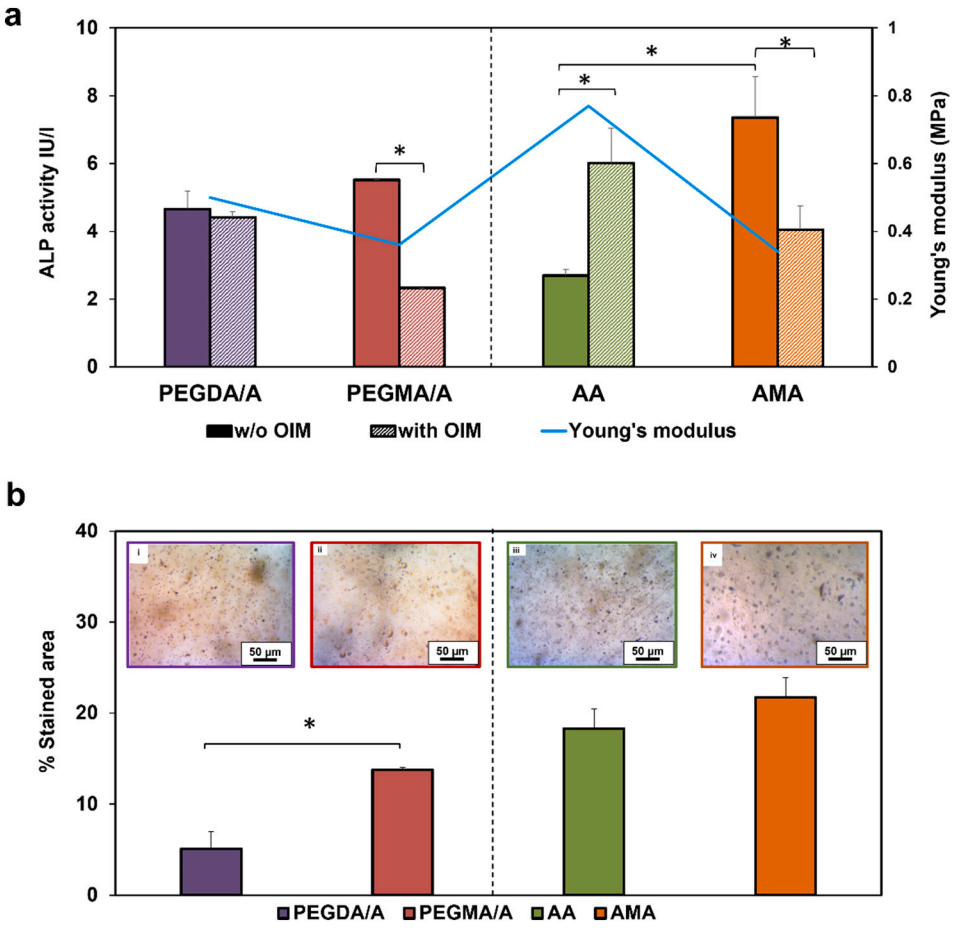

Fig. 7. ALP assay and staining. (a) Quantification of ALP activity on with (w) and without (w/o) OIM groups on week 3 with young's modulus in secondary axis. (b) Quantification of the percentage of ALP-stained area using ImageJ on week 3 w/o OIM group and inset image shows the corresponding optical microscopy images of ALP-stained 3D bioprinted scaffolds on week 3 without (w/o) OIM samples (scale 50 µm). * Indicates the significant difference at $p < 0.05$.

Fig. 7 (b with inset images i–iv) show the ALP staining to be almost uniform across all the samples. The percentage of ALP-stained area was quantified using ImageJ, and it corroborates with the reported assay results (Fig. 7 (b)). AMA shows higher values of the percentage-stained area as compared to the PEG group. The ALP staining intensities are close enough with assay results.

3.7.2. Alizarin red staining

Alizarin red staining for calcium mineralization demonstrated a higher level of calcium deposition in all the scaffolds. UMSCs in all the bioinks are found to produce homogenous calcium deposits throughout the entire scaffold (Fig. 8). Cells in all the bioinks are in different planes since they were enclosed in the hydrogel. Obtained images reveal variation in staining intensity and high intensity-stained area was seen in dark regions. The intense staining of calcium deposition in AA and AMA scaffolds with dark-red hue is shown in Fig. 8 (c and d). The quantification of alizarin red staining using ImageJ is shown in Fig. 8 (d), and it can be noted that PEGMA/A has a larger stained area than PEGDA/A.

3.7.3. Gene expression analysis

Gene expression study revealed positive expression of osteogenic markers in all bioinks without osteogenic induction media (w/o OIM) in week 1 and 3. In comparison to the acrylate groups, ALP was significantly upregulated in methacrylate PEGMA/A and AMA scaffolds (Fig. 9 (a)). In AMA samples, ALP expression increases from week 1 to week 3. On comparing AMA week 1 and week 3 scaffolds with AA week 1, AMA scaffolds had greater levels of RUNX2 expression. In Fig. 9 (b), PEGMA/A week 3 was also shown to be greater than PEGDA/A week 1. Fig. 9 (c) indicates that expression of COL1 was upregulated in methacrylate groups from week 1 to week 3.

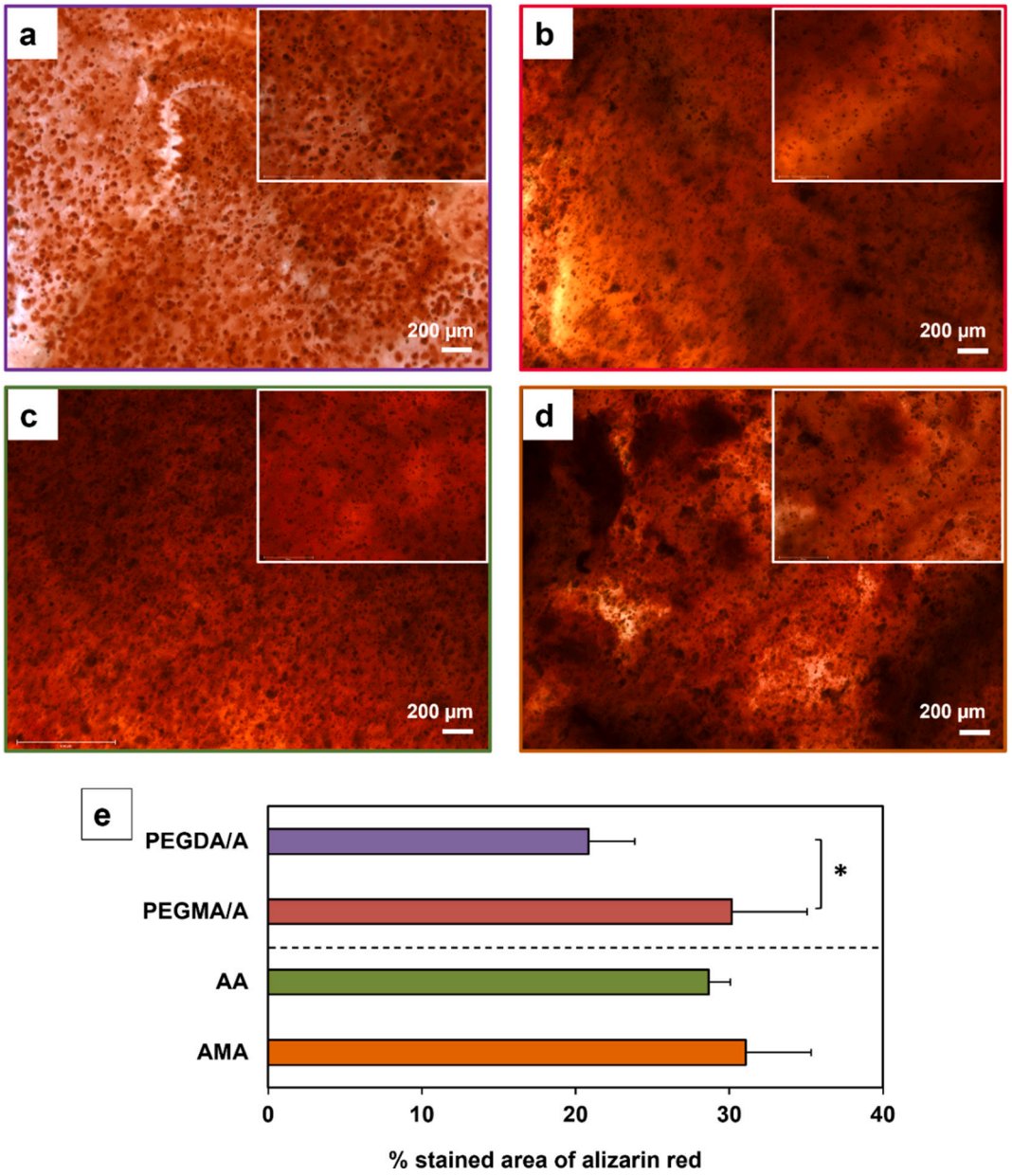

Fig. 8. Representative images of alizarin red staining of UMSCs encapsulated in different bioinks without OIM (w/o OIM) on week 3. 4× images (scale 200 µm). of (a) PEGDA/A, (b) PEGMA/A, (c) AA, (d) AMA with corresponding 10× inset image and (e) Quantification of the percentage of alizarin red stained area using ImageJ on week 3 w/o OIM group. * Indicates the significant difference at $p < 0.05$. (For interpretation of the references to color in this figure legend, the reader is referred to the web version of this article.)

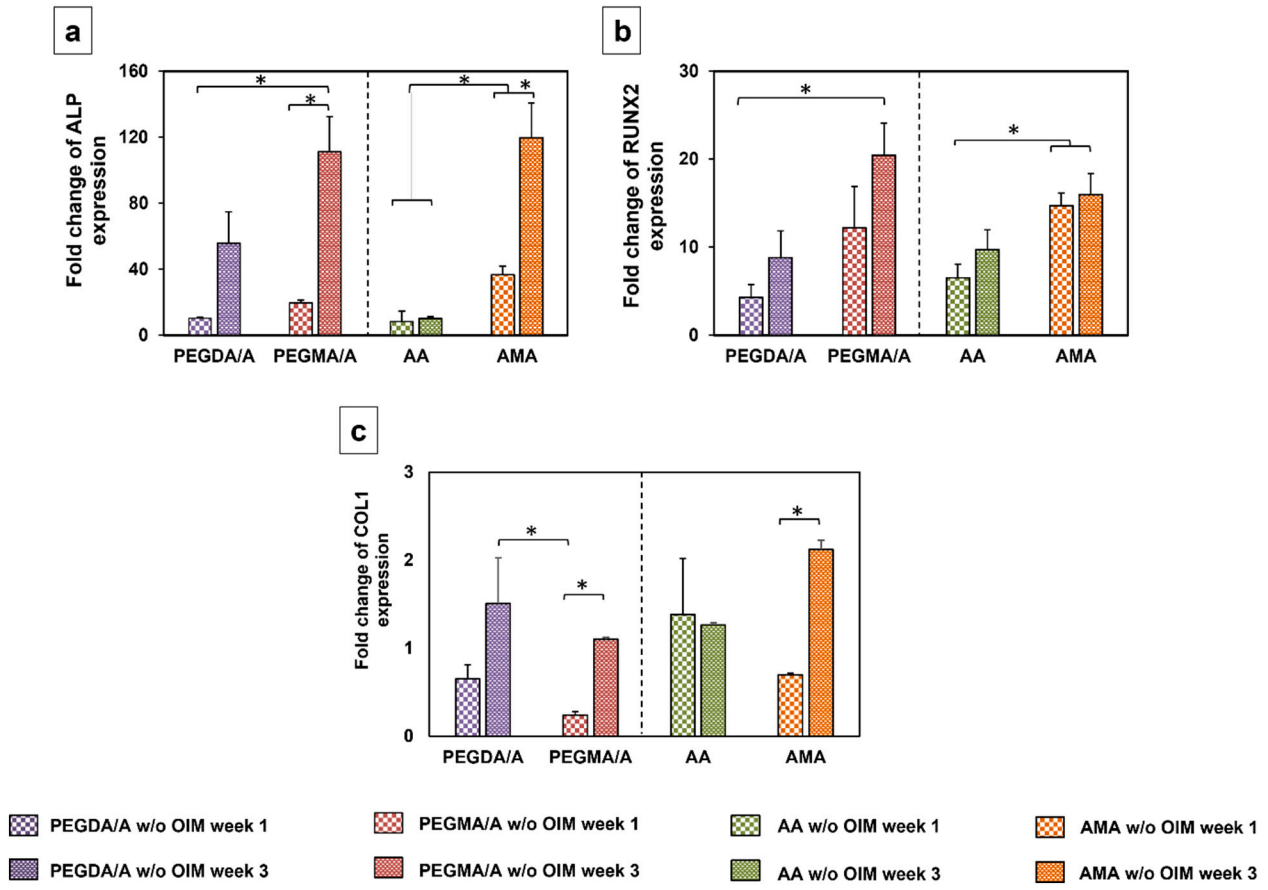

Fig. 9. Quantitative reverse transcription PCR analysis of cell-laden 3D-bioprinted scaffolds at week 1 and 3. (a) ALP, (b) RUNX2 and (c). COL1 expression. * Indicates the significant difference at $p < 0.05$.

4. Discussion

We successfully formulated photo-cross-linkable PEG and sodium alginate with acrylate and methacrylate groups and evaluated their 3D printability. These photo-cross-linked PEG groups demonstrated printability with alginate, as single material did not provide enough viscosity to get an appropriate structure (Supplementary Fig. S4). During 3D bioprinting, the crucial parameter of bioink that needs to be considered is the microenvironment for cell survival. Hydrogel materials have been used for 3D bioprinting due to their ease of printability and to prevent damage to cells while printing [38]. 3D bioprinting is used to fabricate relatively simple structures with single cells or alternate layers of different cells or material, which could mimic the natural architecture of the tissue [6]. Hence validating the photo-cross-linkable hydrogel, which can be 3D printable, has immense application in the fabrication of hybrid scaffolds for bone tissue regeneration. In our study, we have successfully shown the 3D printability, cytocompatibility, and osteogenic differentiation of UMSCs as evident of ALP activity.

The formulated chemical moieties of photo-cross-linkable hydrogels were confirmed using ^{1}H NMR and FTIR characterizations (Supplementary Fig. S1). From ^{1}H MNR, we confirmed the functionalization of acrylate and methacrylate groups (Fig. 3 (a and b)). The mechanical strength of the fabricated scaffolds can be tightly regulated by the crosslinking parameters. The combination of PEG and alginate gradually increases the tensile strength of the 3D printed constructs. Scaffolds crosslinked with both blue light and $CaCl_2$ showed high tensile strength compared to the single cross-linking agent (Fig. 4). The sequence of cross-linking plays a major role in scaffold cross-linking most particularly stabilizing the structure. For example, directly 3D bioprinting on $CaCl_2$ bath blocks the printing head nozzles either cross-linking with $CaCl_2$ solution prior to photo-cross-linking led to the dissolution of PEG components. The dissolution of PEGDA or PEGMA will affect the structural integrity of the scaffold. As a result, we always followed photo-cross-linking and then ionic cross-linking sequence. The ameliorated tensile strength of hydrogels was due to both physical and ionic cross-linking mechanism. Exposure to blue light forms a covalent bond between polymer molecules *via* a free radical mechanism. They were treated with divalent cation $CaCl_2$ solution results in the formation of ionic bonds in the hydrogel system. The improved tensile properties of hydrogels were due to the synergistic effects of covalent and ionic bonds. It was subsequently demonstrated that the extent of cross-linking influences the swelling and degradation properties of the hydrogel that were important for *in vitro* studies of 3D bioprinted scaffolds. The water uptake profile is used to determine the nutrient transfer to the scaffold for cell survival through the diffusive nature of fluid/ions [34]. All the sample groups showed efficient water intake capacity, which depicts appropriate fluid uptake from the surrounding environment (Fig. 5). This can be related to proper nutrient transfer to the encapsulated cells and ensure the cells' survival. Initially, AMA scaffolds showed decrease in size which demonstrates shrinkage of samples due to cation induced cross-linking with $CaCl_2$. Dual cross-linking suppresses the swelling behavior of AMA scaffold and surplus quantity of Ca^{2+} ions in the solution results in shrinking of samples till their presence [15]. Once excess Ca^{2+} ions replaced in the SBF solution the scaffolds start to swell on 48 h (Day 2). On later time points we also observed that AMA samples appear to degrade after 168 h (Day 7) due to the ion-exchange reaction. As stated, ion-exchange reaction happens between the Ca^{2+} ions present in the block of alginate chain and monovalent ions present in the SBF solution [39,40]. Here it is worth mentioning that we also observed the appearance of turbidity of the SBF solution while the scaffolds start to

disintegrate. The degradation capability of AMA samples after 336 h (Day 14) which would aid *in vivo* tissue integration and new tissue formation. The ideal bone-implant should eventually allow new tissue formation during degradation of graft or scaffold over time. The degree of swelling and degradation can be associated with the cross-linking efficiency of hydrogels. The high cross-linking results in less swelling or degradation of hydrogels and *vice versa*. The high swelling or degradation ability of alginate as a natural polymer can be associated with their gradual exchange of ions [41,42]. In this case, we used a photo-cross-linkable hydrogel with sodium alginate, so the swelling of the scaffold might be attributed to non-chemically modified alginate. Additionally, we observed that PEG groups mixed with sodium alginate to improve the printability showed a higher swelling rate as compared to alginate groups.

The influence of cell viability was tested by live/dead staining using FDA and PI fluorescent dye. The fluorescence micrographs on day 1 (Fig. 6 (b)) showed that cells are viable has high cell viability percentage (Supplementary Fig. S6). The cells did not show any spreading morphology indicating they are suspended in the hydrogel system due to lack of RGD group. 3D bioprinting did not significantly influence cell viability. Earlier reports suggested that an increase in cell number over the incubation time was evident in cell proliferation efficiency. Further, to check the cell proliferation on 3D bioprinted we have performed alamar blue dye reduction assay on week 1 and week 3 which indicates that cells are viable and multiplying. The different trend in PEGMA/A without and with OIM scaffolds has been observed but they are not significantly different (Fig. 6 c and Supplementary Fig. S7 a). Similarly, in case of AA samples (Fig. 6 c and d & Supplementary Fig. S7 a and b), there is no statistically significant difference between samples though higher or lower values encountered. The assay value showed a significant increment in AA with OIM on week 3. All the sample groups, except AA, showed similar reduction values at all the corresponding time points. However, cell proliferation increased from week 1 to week 3 in all the scaffolds (Fig. 6 (c and e)). dsDNA content was quantified using picogreen kit assay, and it complied with the alamar blue test results (Fig. 6 (d and f)). An increment in DNA content was observed in all OIM samples after week 1. Week 1 of PEGMA/A with OIM samples showed increased DNA concentration and not in alamar blue (Fig. 6 c and d). This might be due to less metabolic activity at *in vitro* conditions even if the cell number increases [43]. However, the anomalous behavior of the assay can be explored further if needed. In any case, osteoinduction supplements did not influence cell proliferation in our study. On week 3, all the scaffolds showed a similar amount of DNA content, and the reason might be attributed to the initiation of cell differentiation [44]. During cell differentiation, the cell proliferating level attains a straight line and expresses early cell differentiation proteins. Hence, we also ascertained the ALP activity on 3D bioprinted scaffolds with and without OIM at week 3. The ALP activity of samples showed a positive level of ALP expression on all the sample groups. Despite supplements, scaffolds did not show a significant effect on ALP expression. Fig. 7 (a) reveals that the methacrylate group showed increased ALP activity without OIM; this could be a result of material stiffness. When cells are encapsulated in the hydrogel, it might express less, neither extrinsically added induction supplements are not entirely inducing differentiation [45] so with material stiffness w/o OIM sample expresses ALP in our case. However, in our case all the sample groups expressed ALP markers as evidence of osteodifferentiation of UMSCs (Fig. 7). Previous research has suggested that a mechanical cue may overshadow the growth factors' ability to induce differentiation [9,10]. To take forward, the function of mechanical cues and GFs must be explored more on bone tissue regeneration application.

The extent osteogenic differentiation was observed by alizarin red staining and reverse transcription PCR analysis. Mineralization is seen as a sign of osteogenic differentiation [46,47]. Alizarin red can detect calcium deposits in cells, resulting in a red-colored compound. The calcium deposition in all of the sample groups is seen in Fig. 8. When compared to the PEGDA/A group, PEGMA/A showed greater intensity, which supports the quantification results (Fig. 8 (e)). According to the stained images, the intensity of calcium deposition staining was found to be higher in the methacrylate group, but there was no statistical significance in the alginate group. The results of the alizarin red staining match the ALP staining pattern. To further confirm the osteogenic differentiation of UMSCs in hydrogels, a set of osteogenic markers assessed by gene expression analysis. mRNA expression levels were measured on week 1 and week 3 of without OIM samples. ALP enzyme activity was upregulated in methacrylate groups, ALP involves in deposition of minerals on ECM molecules [48] and found to be increasing over time (Fig. 9 (a)). RUNX2 regulates ALP and impacts the differentiation of UMSCs into osteogenesis in the early stages of bone growth [48]. In particular, RUNX2 displayed a homogenous expression in all the conditions (Fig. 9 (b)) which upregulates the ALP activity in 3D bioprinted scaffolds (Fig. 9 (a)). Collagen type 1 is a basic matrix protein produced by osteoblasts that plays a major role in bone cell phenotypic development and contributes to matrix strength [45,48]. COL1 is actively expressed in all the samples and elevated levels of COL1 were noticed in methacrylate groups and found to be raising over time (Fig. 9 (c)). The aforementioned data demonstrates the ability of UMSCs to differentiate into osteolineage in 3D bioprinted scaffolds. It's worth mentioning that we also detected osteogenesis in the presence of material stiffness when no osteogenic differentiation supplements were used.

Numerous studies have shown the degree of cross-linking and mechanical strength influences cell metabolism. Mechanical behavior of PEG and alginate can be varied by varying the concentration of polymers, functionalization, and cross-linker. Photo-functionalized acrylate and methacrylate of PEG and alginate was used for 3D bioprinting which demonstrated distinct tensile strength values. Mechanical testing data has shown that AA has a high Young's modulus of 0.77 MPa when compared to other hydrogel groups (Fig. 4 (f)). Functionalization of alginate with acrylate group increased the mechanical strength of the hydrogel. Acrylate groups have resulted in stiff material properties, while methacrylate groups featured flexibility. Enormous studies reported that the physical cue such as matrix stiffness plays an essential role in stem cell differentiation through mechanotransduction process (Supplementary Table S2). Due to the material's elasticity and topography, cells can sense and transmute into biochemical signals, which could hasten the differentiation of cells into osteogenic lineage [49]. Material elasticity and stiffness can be tuned by altering the polymer chain length, polymer molecular weight/concentration, and cross-linking mechanism. Mesenchymal stem cells in the stiffer hydrogel materials preferentially acquired osteogenesis over adipogenesis. Materials with Young's modulus greater than 25 kPa supported osteogenic differentiation of mesenchymal stem cells. In this study, we reported the mechanical strength of 3D bioprinted scaffolds in terms of Young's modulus. Interestingly, all the groups depict Young's modulus of more than 25 kPa and show osteogenic differentiation. Functionalization of polymer alters material stiffness which has positive impact on cell differentiation. Our work shows that material stiffness alone can direct UMSCs differentiation into the osteogenic lineage. Osteogenic supplements did not significantly influence the cell differentiation on hydrogel encapsulated cells. From our results, we could observe that lowest stiffness shows the highest ALP activity (Fig. 7 (a)) and gene expression profiles (Fig. 9). The observation that AMA with Young's modulus of 0.34 MPa depicts higher levels of ALP in the absence of osteoinduction media. Our results showed that the material stiffness in the range of ~0.3 MPa favored osteo differentiation of mesenchymal stem cells. We could elucidate that differentiation was attributed due to mechanical behavior. Previous reports suggest that MSCs could be differentiated either by biochemical osteogenic factors like BMP-2, FGF-2, and dexamethasone; or by mechanotransduction mechanism for bone tissue engineering applications [24,50–52]. These studies also show that the use of biochemical growth factors can be avoided or decreased in dosage by using the material and mechanical properties to influence the cell fate.

We successfully demonstrated the 3D printability of photo-cross-linked hydrogels, and it has been proven that the bioprinted scaffolds possess osteoinductive nature. So far, the generated results imply that the mechanical property of the scaffold will influence the cell's fate in terms of differentiation. The 3D bioprinted scaffolds showed better biocompatibility and cell proliferation. Chemically modified, these photo-cross-linkable materials demonstrated superior mechanical strength when compared to natural polymers. The attributes of material stiffness influenced the differentiation behavior of UMSCs. Future findings can lead to the new possibility of developing in-house composite materials to avoid variances and to improve bone tissue regeneration by hybrid 3D bioprinting.

5. Conclusions

We have reported the formulation of natural and synthetic polymers with acrylate and methacrylate functional moieties and efficiently photo-cross-linked with visible blue light. These photo-cross-linkable PEG and sodium alginate hydrogels were 3D bioprinted successfully. 3D bioprinting did not significantly influence cell viability. These combinatorial polymers have superior mechanical strength compared to natural polymers, and we showed that all the groups have young's modulus of more than 25 kPa that led to osteolineage, which was confirmed with ALP staining and assay, alizarin red staining and gene expression analysis. In our study, considering minimalistic materials and without the addition of any supplements for 3D bioprinting to enhance bone tissue regeneration. Hence, these findings will help us in the development of composite ink or layer-by-layer printing of different inks, likely alternate layers of hydrogel and ceramic. In the future, fabricating cages like hybrid scaffolds with outer porous ceramic architecture and inner cells encapsulated hydrogel system will elicit better tissue integration and cell differentiation while providing load support.

CRediT authorship contribution statement

Meenakshi Kamaraj: Conceptualization, Investigation, Methodology, Formal analysis, Validation, Writing-Original draft preparation.

Sreevani Gaddamedi: Conceptualization, Investigation, Methodology, Formal analysis, Writing-Reviewing.

Ganesan Prabusankar: Formal analysis, Writing-Reviewing and Editing

Subha Narayan Rath: Conceptualization, Supervision, Writing-Reviewing and Editing, Funding acquisition, Project administration, Resources.

Declaration of competing interest

The authors declare that they have no known competing financial interests or personal relationships that could have appeared to influence the work reported in this paper.

Acknowledgment

The authors would like to acknowledge the Department of Biotechnology (DBT- BT/PR13381/MED/32/509/2015), Ministry of Human Resource and Development (MHRD), DBT-Research Assistance project scheme (DBT/RA/2018-20). Authors also like to acknowledge Mr. Pravin Shankar Giri for the help with RT-qPCR study.

Appendix A. Supplementary data

Supplementary data to this article can be found online at https://doi.org/10.1016/j.msec.2021.112478.

References

[1] S.N. Rath, A. Brandl, D. Hiller, A. Hoppe, U. Gbureck, R.E. Horch, A.R. Boccaccini, U. Kneser, Bioactive copper-doped glass scaffolds can stimulate endothelial cells in co-culture in combination with mesenchymal stem cells, PLoS One 9 (2014) 1–24, https://doi.org/10.1371/journal.pone.0113319.

[2] T.S. Jang, H. Do Jung, H.M. Pan, W.T. Han, S. Chen, J. Song, 3D printing of hydrogel composite systems: recent advances in technology for tissue engineering, Int. J. Bioprinting 4 (2018) 1–28, https://doi.org/10.18063/IJB.v4i1.126.

[3] F.A. Probst, R. Fliefel, E. Burian, M. Probst, M. Eddicks, M. Cornelsen, C. Riedl, H. Seitz, A. Aszódi, M. Schieker, S. Otto, Bone regeneration of minipig mandibular defect by adipose derived mesenchymal stem cells seeded tri-calcium phosphate-poly(D, L-lactide-co-glycolide) scaffolds, Sci. Rep. 10 (2020) 1–16, https://doi.org/10.1038/s41598-020-59038-8.

[4] J.J. Li, M. Ebied, J. Xu, H. Zreiqat, Current approaches to bone tissue engineering: the interface between biology and engineering, Adv. Healthc. Mater. 7 (2018) 1–8, https://doi.org/10.1002/adhm.201701061.

[5] S.J. and M. Guvendiren, 3D printed wavy scaffolds enhance mesenchymal stem cell osteogenesis, Micromachines 11 (2020), https://doi.org/10.3390/mi11010031.

[6] N. Ashammakhi, S. Ahadian, C. Xu, H. Montazerian, H. Ko, R. Nasiri, N. Barros, A. Khademhosseini, Bioinks and bioprinting technologies to make heterogeneous and biomimetic tissue constructs, Mater. Today Bio. 1 (2019), https://doi.org/10.1016/j.mtbio.2019.100008.

[7] S. Van Belleghem, L. Torres, M. Santoro, B. Mahadik, A. Wolfand, P. Kofinas, J. P. Fisher, Hybrid 3D printing of synthetic and cell-laden bioinks for shape retaining soft tissue grafts, Adv. Funct. Mater. 30 (2020) 1–10, https://doi.org/10.1002/adfm.201907145.

[8] Y. He, F. Yang, H. Zhao, Q. Gao, B. Xia, J. Fu, Research on the printability of hydrogels in 3D bioprinting, Sci. Rep. 6 (2016) 1–13, https://doi.org/10.1038/srep29977.

[9] G. Choe, S. Oh, J.M. Seok, S.A. Park, J.Y. Lee, Graphene oxide/alginate composites as novel bioinks for three-dimensional mesenchymal stem cell printing and bone regeneration applications, Nanoscale 11 (2019) 23275–23285, https://doi.org/10.1039/c9nr07643c.

[10] M.T. Poldervaart, B. Goversen, M. De Ruijter, A. Abbadessa, F.P.W. Melchels, F. C. Öner, W.J.A. Dhert, T. Vermonden, J. Alblas, 3D bioprinting of methacrylated hyaluronic acid (MeHA) hydrogel with intrinsic osteogenicity, PLoS One 12 (2017) 1–15, https://doi.org/10.1371/journal.pone.0177628.

[11] A. Leucht, A.C. Volz, J. Rogal, K. Borchers, P.J. Kluger, Advanced gelatin-based vascularization bioinks for extrusion-based bioprinting of vascularized bone equivalents, Sci. Rep. 10 (2020) 1–15, https://doi.org/10.1038/s41598-020-62166-w.

[12] M.M. Stanton, J. Samitier, S. Sánchez, Bioprinting of 3D hydrogels, Lab Chip 15 (2015) 3111–3115, https://doi.org/10.1039/c5lc90069g.

[13] W. Zhou, H. Zhang, Y. Liu, X. Zou, J. Shi, Y. Zhao, Y. Ye, Y. Yu, J. Guo, Sodium alginate-polyethylene glycol diacrylate based double network fiber: rheological properties of fiber forming solution with semi-interpenetrating network structure, Int. J. Biol. Macromol. 142 (2020) 535–544, https://doi.org/10.1016/j.ijbiomac.2019.09.125.

[14] S. Pramanik, F. Ataollahi, B. Pingguan-Murphy, A.A. Oshkour, N.A.A. Osman, In vitro study of surface modified poly(ethylene glycol)-impregnated sintered bovine bone scaffolds on human fibroblast cells, Sci. Rep. 5 (2015) 1–11, https://doi.org/10.1038/srep09806.

[15] J.H.G.S. Shengzhong Zhou, Alexander Bismarcka, Ion-responsive alginate based macroporous injectable hydrogel scaffolds prepared by emulsion templating, J. Mater. Chem. C 3 (2015) 10715–10722, https://doi.org/10.1039/b000000x.

[16] A.R. Liberski, Three-dimensional printing of alginate: from seaweeds to heart valve scaffolds, QScience Connect. 2016 (2016) 3, https://doi.org/10.5339/connect.2016.3.

[17] P. Karami, C.S. Wyss, A. Khoushabi, A. Schmocker, M. Broome, C. Moser, P. E. Bourban, D.P. Pioletti, Composite double-network hydrogels to improve adhesion on biological surfaces, ACS Appl. Mater. Interfaces 10 (2018) 38692–38699, https://doi.org/10.1021/acsami.8b10735.

[18] J.A. Killion, L.M. Geever, D.M. Devine, J.E. Kennedy, C.L. Higginbotham, Mechanical properties and thermal behaviour of PEGDMA hydrogels for potential bone regeneration application, J. Mech. Behav. Biomed. Mater. 4 (2011) 1219–1227, https://doi.org/10.1016/j.jmbbm.2011.04.004.

[19] C.A. Verheyen, L. Morales, J. Sussman, K. Paunovska, V. Manzoli, N.M. Ziebarth, A. A. Tomei, Characterization of polyethylene glycol-reinforced alginate microcapsules for mechanically stable cell immunoisolation, Macromol. Mater. Eng. 304 (2019) 1–11, https://doi.org/10.1002/mame.201800679.

[20] G. Yang, Z. Xiao, H. Long, K. Ma, J. Zhang, X. Ren, J. Zhang, Assessment of the characteristics and biocompatibility of gelatin sponge scaffolds prepared by various crosslinking methods, Sci. Rep. 8 (2018) 1–13, https://doi.org/10.1038/s41598-018-20006-y.

[21] J.B. Rose, S. Pacelli, A.J. El Haj, H.S. Dua, A. Hopkinson, L.J. White, F.R.A.J. Rose, Gelatin-based materials in ocular tissue engineering, Materials (Basel) 7 (2014) 3106–3135, https://doi.org/10.3390/ma7043106.

[22] W. Hu, Z. Wang, Y. Xiao, S. Zhang, J. Wang, Advances in crosslinking strategies of biomedical hydrogels, Biomater. Sci. 7 (2019) 843–855, https://doi.org/10.1039/c8bm01246f.

[23] K.S. Lim, B.J. Klotz, F.P.W.M. Gabriella, C.J. Lindberg, Gary, J. Hooper, T.B.F. W. Jos Malda, Debby Gawlitta, Visible light crosslinking of gelatin hydrogels offers an enhanced cell microenvironment with improved light penetration depth, Macromol. Biosci. (2019) 1–37, https://doi.org/10.1002/mabi.201900098.

[24] R.K. Das, V. Gocheva, R. Hammink, O.F. Zouani, A.E. Rowan, Stress-stiffening-mediated stem-cell commitment switch in soft responsive hydrogels, Nat. Mater. 15 (2016) 318–325, https://doi.org/10.1038/nmat4483.
[25] M. Witkowska-Zimny, K. Walenko, E. Wrobel, P. Mrowka, A. Mikulska, J. Przybylski, Effect of substrate stiffness on the osteogenic differentiation of bone marrow stem cells and bone-derived cells, Cell Biol. Int. 37 (2013) 608–616, https://doi.org/10.1002/cbin.10078.
[26] K.H. Vining, D.J. Mooney, Mechanical forces direct stem cell behaviour in development and regeneration, Nat. Rev. Mol. Cell Biol. 18 (2017) 728–742, https://doi.org/10.1038/nrm.2017.108.
[27] T. Zhang, S. Lin, X. Shao, Q. Zhang, C. Xue, S. Zhang, Y. Lin, B. Zhu, X. Cai, Effect of matrix stiffness on osteoblast functionalization, Cell Prolif. 50 (2017) 1–9, https://doi.org/10.1111/cpr.12338.
[28] R.O. Navarrete, E.M. Lee, K. Smith, S.L. Hyzy, M. Doroudi, J.K. Williams, K. Gall, B. D. Boyan, Z. Schwartz, Substrate stiffness controls osteoblastic and chondrocytic differentiation of mesenchymal stem cells without exogenous stimuli, PLoS One 12 (2017) 1–18, https://doi.org/10.1371/journal.pone.0170312.
[29] Y. Liu, Z. Li, J. Li, S. Yang, Y. Zhang, B. Yao, W. Song, X. Fu, S. Huang, Stiffness-mediated mesenchymal stem cell fate decision in 3D-bioprinted hydrogels, Burn. Trauma. 8 (2020) 1–13, https://doi.org/10.1093/burnst/tkaa029.
[30] L. Cai, J. Lu, V. Sheen, S. Wang, Promoting nerve cell functions on hydrogels grafted with poly(l-lysine), Biomacromolecules 13 (2012) 342–349, https://doi.org/10.1021/bm201763n.
[31] J.A. Burdick, C. Chung, X. Jia, M.A. Randolph, R. Langer, Controlled degradation and mechanical behavior of photopolymerized hyaluronic acid networks, Biomacromolecules 6 (2005) 386–391, https://doi.org/10.1021/bm049508a.
[32] F. Paquin, J. Rivnay, A. Salleo, N. Stingelin, C. Silva, Multi-phase semicrystalline microstructures drive exciton dissociation in neat plastic semiconductors, J. Mater. Chem. C 3 (2015) 10715–10722, https://doi.org/10.1039/b000000x.
[33] S.D. Eswaramoorthy, N. Dhiman, G. Korra, C.M. Oranges, D.J. Schaefer, S.N. Rath, S. Madduri, Isogenic-induced endothelial cells enhance osteogenic differentiation of mesenchymal stem cells on silk fibroin scaffold, Regen. Med. 14 (2019) 647–661, https://doi.org/10.2217/rme-2018-0166.
[34] B. Sarker, R. Singh, R. Silva, J.A. Roether, J. Kaschta, R. Detsch, D.W. Schubert, I. Cicha, A.R. Boccaccini, Evaluation of fibroblasts adhesion and proliferation on alginate-gelatin crosslinked hydrogel, PLoS One 9 (2014) 1–12, https://doi.org/10.1371/journal.pone.0107952.
[35] H. Yang, S. Chen, L. Liu, C. Lai, X. Shi, Synthesis, characterization and osteogenesis of phosphorylated methacrylamide chitosan hydrogels, RSC Adv. 8 (2018) 36331–36337, https://doi.org/10.1039/c8ra05378b.
[36] S. Sankar, M. Kakunuri, S.D. Eswaramoorthy, C.S. Sharma, S.N. Rath, Effect of patterned electrospun hierarchical structures on alignment and differentiation of mesenchymal stem cells: biomimicking bone, J. Tissue Eng. Regen. Med. 12 (2018) e2073–e2084, https://doi.org/10.1002/term.2640.
[37] S.N. Rath, L.A. Strobel, A. Arkudas, J.P. Beier, A.K. Maier, P. Greil, R.E. Horch, U. Kneser, Osteoinduction and survival of osteoblasts and bone-marrow stromal cells in 3D biphasic calcium phosphate scaffolds under static and dynamic culture conditions, J. Cell. Mol. Med. 16 (2012) 2350–2361, https://doi.org/10.1111/j.1582-4934.2012.01545.x.
[38] D.F. Duarte Campos, A. Blaeser, K. Buellesbach, K.S. Sen, W. Xun, W. Tillmann, H. Fischer, Bioprinting organotypic hydrogels with improved mesenchymal stem cell remodeling and mineralization properties for bone tissue engineering, Adv. Healthc. Mater. 5 (2016) 1336–1345, https://doi.org/10.1002/adhm.201501033.
[39] A. Kirillova, R. Maxson, G. Stoychev, C.T. Gomillion, L. Ionov, 4D biofabrication using shape-morphing hydrogels, Adv. Mater. 29 (2017) 1–8, https://doi.org/10.1002/adma.201703443.
[40] S.K. Bajpai, R. Tankhiwale, Investigation of water uptake behavior and stability of calcium alginate/chitosan bi-polymeric beads: part-1, React. Funct. Polym. 66 (2006) 645–658, https://doi.org/10.1016/j.reactfunctpolym.2005.10.017.
[41] M. Govindharaj, U.K. Roopavath, S.N. Rath, Valorization of discarded marine eel fish skin for collagen extraction as a 3D printable blue biomaterial for tissue engineering, J. Clean. Prod. 230 (2019) 412–419, https://doi.org/10.1016/j.jclepro.2019.05.082.
[42] L. Benning, L. Gutzweiler, K. Tröndle, J. Riba, R. Zengerle, P. Koltay, S. Zimmermann, G.B. Stark, G. Finkenzeller, Assessment of hydrogels for bioprinting of endothelial cells, J. Biomed. Mater. Res. A 106 (2018) 935–947, https://doi.org/10.1002/jbm.a.36291.
[43] V.M.C. Quent, D. Loessner, T. Friis, J.C. Reichert, D.W. Hutmacher, Discrepancies between metabolic activity and DNA content as tool to assess cell proliferation in cancer research, J. Cell. Mol. Med. 14 (2010) 1003–1013, https://doi.org/10.1111/j.1582-4934.2010.01013.x.
[44] Aldo R. Boccaccini, Ulrich Kneser, Subha N. Rath, Patcharakamon Nooeaid, Andreas Arkudas, Justus P. Beier, Leonie A. Strobel, Andreas Brandl, Judith A. Roether, Raymund E. Horch, Adipose- and bone marrow-derived mesenchymal stem cells display different osteogenic differentiation patterns in 3D bioactive glass-based scaffolds Subha, J. Tissue Eng. Regen. Med. 12 (2013) 181–204, https://doi.org/10.1002/term.
[45] S.D. Eswaramoorthy, N. Dhiman, A. Joshi, S.N. Rath, 3D bioprinting of mesenchymal stem cells and endothelial cells in an alginate-gelatin-based bioink, J. 3D Print. Med. 5 (2021) 23–36, https://doi.org/10.2217/3dp-2020-0026.
[46] S.D. Eswaramoorthy, S. Bethapudi, S.I. Almelkar, S.N. Rath, Regional differentiation of adipose-derived stem cells proves the role of constant electric potential in enhancing bone healing, J. Med. Biol. Eng. 38 (2018) 804–815, https://doi.org/10.1007/s40846-018-0373-2.
[47] J. Jeon, M.S. Lee, H.S. Yang, Differentiated osteoblasts derived decellularized extracellular matrix to promote osteogenic differentiation, Biomater. Res. 22 (2018) 1–9, https://doi.org/10.1186/s40824-018-0115-0.
[48] A. Polini, D. Pisignano, M. Parodi, R. Quarto, S. Scaglione, Osteoinduction of human mesenchymal stem cells by bioactive composite scaffolds without supplemental osteogenic growth factors, PLoS One 6 (2011) 1–8, https://doi.org/10.1371/journal.pone.0026211.
[49] M. d'Angelo, E. Benedetti, M.G. Tupone, M. Catanesi, V. Castelli, A. Antonosante, A. Cimini, The role of stiffness in cell reprogramming: a potential role for biomaterials in inducing tissue regeneration, Cells 8 (2019), https://doi.org/10.3390/cells8091036.
[50] M. Dang, L. Saunders, X. Niu, Y. Fan, P.X. Ma, Biomimetic delivery of signals for bone tissue engineering, Bone Res. 6 (2018), https://doi.org/10.1038/s41413-018-0025-8.
[51] A. Paul, V. Manoharan, D. Krafft, A. Assmann, J.A. Uquillas, S.R. Shin, A. Hasan, M. A. Hussain, A. Memic, A.K. Gaharwar, A. Khademhosseini, Nanoengineered biomimetic hydrogels for guiding human stem cell osteogenesis in three dimensional microenvironments, J. Mater. Chem. B 4 (2016) 3544–3554, https://doi.org/10.1039/c5tb02745d.
[52] F.E. Freeman, D.J. Kelly, Tuning alginate bioink stiffness and composition for controlled growth factor delivery and to spatially direct MSC fate within bioprinted tissues, Sci. Rep. 7 (2017) 1–12, https://doi.org/10.1038/s41598-017-17286-1.